Journal of Biomechanics 49 (2016) 193–204

Contents lists available at ScienceDirect

Journal of Biomechanics

journal homepage: www.elsevier.com/locate/jbiomech
www.JBiomech.com

Low-density lipoprotein transport through an arterial wall under hyperthermia and hypertension conditions – An analytical solution

Marcello Iasiello [a,b], Kambiz Vafai [a,*], Assunta Andreozzi [b], Nicola Bianco [b]

[a] Department of Mechanical Engineering, University of California, Riverside, CA 92521, USA
[b] Dipartimento di Ingegneria Industriale, Università degli Studi di Napoli Federico II, P.le Tecchio, 80, Napoli 80125, Italy

ARTICLE INFO

Article history:
Accepted 3 December 2015

Keywords:
Hyperthermia
Hypertension
Low-Density Lipoprotein
Analytical Solution

ABSTRACT

An analytical solution for Low-Density Lipoprotein transport through an arterial wall under hyperthermia conditions is established in this work. A four-layer model is used to characterize the arterial wall. Transport governing equations are obtained as a combination between Staverman–Kedem–Katchalsky membrane equations and volume-averaged porous media equations. Temperature and solute transport fields are coupled by means of Ludwig-Soret effect. Results are in excellent agreement with numerical and analytical literature data under isothermal conditions, and with numerical literature data for the hyperthermia case. Effects of hypertension combined with hyperthermia, are also analyzed in this work.

1. Introduction

The formation of an atherosclerotic plaque inside the wall of an artery is a very dangerous phenomenon for the human health. Computational fluid dynamic has a very important role in the prediction of such phenomena (Abraham et al., 2008), also for other similar phenomena such as aneurysms (Naughton et al., 2014), in which modeling fluid-structure interactions is a primary task (Chung and Vafai, 2012; Sun et al., 2015). If this plaque breaks, a thrombous in the blood vessel occurs, causing vascular obstruction. The thrombous is the cause of many cardiovascular diseases, like strokes and heart attack. The growth of this atherosclerotic plaque is caused by the infiltration of Low-Density Lipoprotein (LDL) through the wall. The LDLs derive from triglycerides hydrolysis of Intermediate-Density Lipoproteins (IDLs) which are not metabolized by the liver. When LDL infiltrates in the intima layer through the endothelium, it can oxidize, attracting monocytes. These monocytes absorb ox-LDL, forming foam cells. Smooth Muscle Cells (SMC) are then prone to move from the tunica media to the intima, promoting the growth of the foam cells that are going to form the plaque. The process of the plaque formation is characterized by the growth of a fibrous connective tissue layer, namely the fibrous cap, that has an important role in calcifying atherosclerotic plaques. The plaque formation can be either stable or unstable. When the plaque is stable, the fibrous cap is thick and solid. In this case, the risk consists in the occlusion of the artery. However, because the growth of the plaque is relative slow, a collateral circulation can occur. On the other hand, an unstable plaque is more dangerous, because it can break, forming a thrombous. In that case, there is no collateral circulation that compensates the problem. When the artery becomes occluded, the reduction of blood flow could cause several fatal problems. For example, an ischemic stroke occurs when blood perfusion of the brain is diminished by a thrombous or by a vascular lumen restriction caused by a growing plaque. Among the various techniques used to counteract such phenomena, an example of emerging therapy for the treatment of LDL is the LDL-apheresis (McGowan, 2013), that reminds of dialysis, in which modeling mass transfer through the vascular access has a primary role. A generic mass transfer model for vascular access was presented by Chelikani et al. (2011). The study of the mechanisms that regulate LDL accumulation through the wall is then extremely important, due to its primary role in the growth of the atherosclerotic plaque.

Following Iasiello et al. (2015), two methods are used to investigate LDL transport through an arterial wall: the first is based on experiments on animals (Meyer et al., 1996; Xie et al., 2013), and the second on predictions. Predictive models can also be distinguished in models based on realistic arteries (Kenjereš and de Loor, 2014) and on idealized arteries (Prosi et al., 2005; Yang and Vafai, 2006; Ai and Vafai, 2006) Depending on how much in detail the wall is represented, predictive methods can also be divided into three categories (Prosi et al., 2005): wall-free models, in which the arterial wall is represented by means of a boundary condition (Wada and Karino, 2000), fluid-wall models, that are also used for other similar transport problems such as the

* Corresponding author.
E-mail address: vafai@engr.ucr.edu (K. Vafai).

http://dx.doi.org/10.1016/j.jbiomech.2015.12.015
0021-9290/

Nomenclature

A	Particular solution polynomial
$\mathbf{B}$	Coefficients matrix
c	LDL concentration (mol/m^3)
c_1, c_2	Constant coefficients
c_f	Heat capacity (J/kg K)
D	LDL mass diffusivity (m^2/s)
Da	Darcy number
$\mathbf{e}$	Known terms vector
f	Inertial coefficient
$\mathbf{g}$	Unknowns vector
$\mathbf{j}$	Mass flux (mol/m^2 s)
k	First-order reaction coefficient (1/s)
k_T	Thermal-diffusion coefficient
K	Hydraulic permeability (m^2)
L	Length (m)
Le	Lewis number
M	Molecular weight (g/mol)
p	Hydraulic pressure (mmHg)
Pe	Mass Peclet number
$\mathbf{q}$	Heat flux (W/m^2)
R	Hydraulic resistance
R_g	Universal gas constant (J/mol K)
Re	Reynolds number
t	Time (s)
T	Temperature (K)
v	Filtration velocity (m/s)
$\mathbf{v}$	Velocity vector (m/s)
y	Radial direction coordinate (m)
z	Axial direction coordinate (m)

Greek letters

α	Thermal diffusivity (m^2/s)
Δ	Difference
ε	Porosity
λ	Thermal conductivity (W/m K)
$\lambda_{1,2}$	Eigenvalues
μ	Dynamic viscosity (kg/m s)
ρ	Density (kg/m^3)
σ	Reflection coefficient

Superscripts

end	Endothelium
i	i-layer
IEL	Internal Elastic Lamina
int	Intima
med	Media
T	Thermal
$*$	Dimensionless

Subscripts

0	Reference
a	Advective
c	Cold
D	Diffusive
eff	Effective property
f	Fluid (plasma) property
h	Hot
ho	Homogeneous
M	Mean
osm	Osmotic
p	Particular
S	Staverman filtration
T	Thermo-diffusive

Other symbols

∇	Nabla
∂	Partial differential
d	Differential
$\langle\rangle$	Volume average of a variable

penetration of liquid medication through an arterial wall (Abraham et al., 2013), in which an homogeneous layer represents the arterial wall (Stangeby and Ethier, 2002), and multi-layer model, in which the heterogeneity of the wall layers is taken into account (Yang and Vafai, 2006; Ai and Vafai, 2006).

Most of the predictive models are based on numerical simulations. Because of the complexity of the problem, only few analytical solutions for comparisons with numerical models based on the multi-layer model were obtained during the years. The first analytical solution for the LDL transport through a straight artery was developed by Yang and Vafai (2008). They obtained flow fields and LDL concentration profiles along the wall radius, considering a simplified one-dimensional case. They used several assumptions to obtain the analytical solution, however, comparisons with literature data showed that their results were quite accurate. A comprehensive solution was presented by Khakpour and Vafai (2008) and Wang and Vafai (2013), using the method of matched asymptotic expansions in conjunction with Laplace transformation to calculate fluid flow fields and LDL distributions. Their results matched the literature data. Effects due to the insertion of a stent were analytically analyzed by Wang and Vafai (2013), showing how stent compactness affects transport phenomena. A model for the transport of therapeutic drugs through a pressurized balloon, was also proposed by Stark et al. (2013). Curvature effects of an artery were exhaustively analytically analyzed by Wang and Vafai (2015). In their study they demonstrate that low curvature ratio increases concentration polarization, i.e. the accumulation of solute on a membrane surface (Colton et al., 1972), at the lumen/endothelium interface.

When hyperthermia occurs in the human body, temperature gradients are generated. This hyperthermia can occur naturally or artificially, for example for the treatment of some diseases like arrhythmias or cancer (Soares et al., 2012; Roesch and Mueller-Huebenthal, 2015; Hernàndez et al., 2015). Predictions of heat transfer during hyperthermia treatments were carried out by Mahjoob and Vafai (2009), Alamiri et al. (2014) and by Wang et al. (2015). Hyperthermia can be induced also with laser angioplasty, that is a technique used to remove plaques. The mass transfer is influenced by temperature gradients by means of Ludwig-Soret effect (Ludwig, 1856; Soret, 1879). When temperature gradients are applied to a solution, the solute tends to move from the hot to the cold zone of the solution (Platten, 2006). The counter part for the effects of mass transfer on temperature is the Dufour effect (Ingle and Horne, 1973). Numerical studies for the LDL transport through the arterial wall under hyperthermia load, applied either from the exterior or the interior of the artery, were recently performed by Chung and Vafai (2014) for a straight artery, and by Iasiello et al. (2015) for a stenosed artery. There are no analytical

results in literature for the comparisons of the cited numerical models describing or predicting hyperthermia effects on LDL transport through an arterial wall.

An analytical solution is established here for the LDL transport through the arterial wall, under hyperthermia conditions. Mass, momentum and energy dimensionless governing equations are solved for both external and internal hyperthermia loads. Comparisons with numerical and analytical results from literature are presented. Effects of hyperthermia, set of thermophysical properties and media/adventitia boundary condition, are also discussed.

2. Mathematical model

2.1. Geometry of an artery: the multi-layer model

The sketch of the arterial wall is shown in Fig. 1a. The space in which the blood flows is called the lumen. The lumen is in direct contact with a layer of cells elongated in the blood flow direction, namely the endothelium, that is a semi-selective barrier which has a primary role into the mass exchanges between the lumen and the rest of the wall. This layer is covered by the glycolcalyx, that is a coating of molecules rich in carbohydrates. After the endothelium, the tunica intima is a layer formed by proteoglycan fibers and looser-thicker collagen fibers, in which LDL tends to accumulate before and during the evolution of the atherosclerotic plaque. The tunica media is a layer made up by connective tissue and smooth muscle cells, that migrates into the intima layer to contribute the growth of the plaque. The last layer is the tunica adventitia, made of connective tissue, in which lymphatic vessels and vasa vasorum are present. Thickness of the arterial wall layers are shown in Fig. 1a.

2.2. Governing equations

The arterial wall is modeled following the multi-layer model (Yang and Vafai, 2006; Ai and Vafai, 2006). Four layers are considered: endothelium, intima, IEL and media, reported in Fig. 1a with their corresponding thicknesses. The glycocalyx layer is neglected in the present study (Tarbell, 2003; Yang and Vafai, 2006; Liu et al., 2011). Tunica adventitia can be replaced by a boundary condition on the media/adventitia interface (Yang and Vafai, 2006; Ai and Vafai, 2006; Yang and Vafai, 2008).

Because in the present study Ludwig-Soret and Dufour effects on LDL transport are considered (Chapman and Cowling, 1952; Wakeham et al., 1991; Kays and Crawford, 1993; Chung and Vafai, 2014; Iasiello et al., 2015), the mass and the heat fluxes $\mathbf{j}$ and $\mathbf{q}$ due to these effects can be in general expressed as a sum of advective, diffusive and thermo-diffusive contributions, respectively $\mathbf{j_a}$, $\mathbf{j_D}$ and $\mathbf{j_T}$ for the mass flux and $\mathbf{q_a}$, $\mathbf{q_D}$ and $\mathbf{q_T}$ for the heat flux:

$$\mathbf{j}=\mathbf{j_a}+\mathbf{j_D}+\mathbf{j_T}=\mathbf{v}c-D_{eff}\nabla c-\frac{k_T\rho_f}{M_f}\frac{D_{eff}}{T}\nabla T \tag{1}$$

$$\mathbf{q}=\mathbf{q_a}+\mathbf{q_D}+\mathbf{q_T}=\mathbf{v}T-\lambda_{eff}\nabla T-\frac{R_gTk_T\rho_f}{M_f}\frac{D_{eff}}{c}\nabla c \tag{2}$$

where $\mathbf{v}$ is the velocity vector, c the solute concentration, D_{eff} the effective solute mass diffusion coefficient, k_T the thermal-diffusion coefficient, ρ_f the plasma density, M_f the plasma molecular weight, T the temperature, λ_{eff} the effective thermal diffusivity and R_g is the universal gas constant. Governing equations for mass, momentum, energy and LDL species are obtained as a combination between Staverman–Kedem–Katchalsky biological membranes equations (Kedem and Katchalsky, 1958) and porous media equations, including Eqs. (1) and (2). Local Thermal Equilibrium (LTE) between the two phases of the porous medium is assumed (Amiri and Vafai, 1994; Nield and Kuznetsov, 1999, 2001; Alazmi and Vafai, 2001):

$$\nabla\cdot\langle\mathbf{v}\rangle=0 \tag{3}$$

$$\frac{\rho_f}{\varepsilon}\left(\frac{\partial\langle\mathbf{v}\rangle}{\partial t}+\langle\mathbf{v}\rangle\cdot\nabla\langle\mathbf{v}\rangle\right)+\nabla\langle p\rangle_f=\frac{\mu_f}{\varepsilon}\nabla^2\langle\mathbf{v}\rangle-\frac{\mu_f}{K}\langle\mathbf{v}\rangle-\frac{\rho_f f}{K^{1/2}}|\langle\mathbf{v}\rangle|\langle\mathbf{v}\rangle+R_g\langle T\rangle\sigma_{osm}\nabla\langle c\rangle \tag{4}$$

$$\frac{\partial\langle c\rangle}{\partial t}+(1-\sigma_S)\langle\mathbf{v}\rangle\cdot\nabla\langle c\rangle=D_{eff}\nabla^2\langle c\rangle+\frac{k_T\rho_f}{M_f}\frac{D_{eff}}{\langle T\rangle}\nabla^2\langle T\rangle-k\langle c\rangle \tag{5}$$

$$\frac{\partial\langle T\rangle}{\partial t}+\langle\mathbf{v}\rangle\cdot\nabla\langle T\rangle=\alpha_{eff}\nabla^2\langle T\rangle+\frac{R_g\langle T\rangle k_T}{c_fM_f}\frac{D_{eff}}{\langle c\rangle}\nabla^2\langle c\rangle \tag{6}$$

where ε is the porosity, t the time, p the pressure, μ_f the plasma dynamic viscosity, K the hydraulic permeability, f the inertial coefficient, σ_{osm} the osmotic reflection coefficient, σ_S the filtration reflection coefficient, k the first-order reaction coefficient, α_{eff} the effective thermal diffusivity, and c_f is the plasma thermal capacity. The last term on the right side of Eq. (4) takes into account osmosis effects. In Eq. (5), the term $(1-\sigma_S)$ takes into account the LDL selective rejection of the membranes. On the right side, the last term models the uptake of solutes operated by SMC and macrophages into the media layer (Fry, 1985; Huang and Tarbell, 1997; Yang and Vafai, 2006; Chung and Vafai, 2012). The symbols

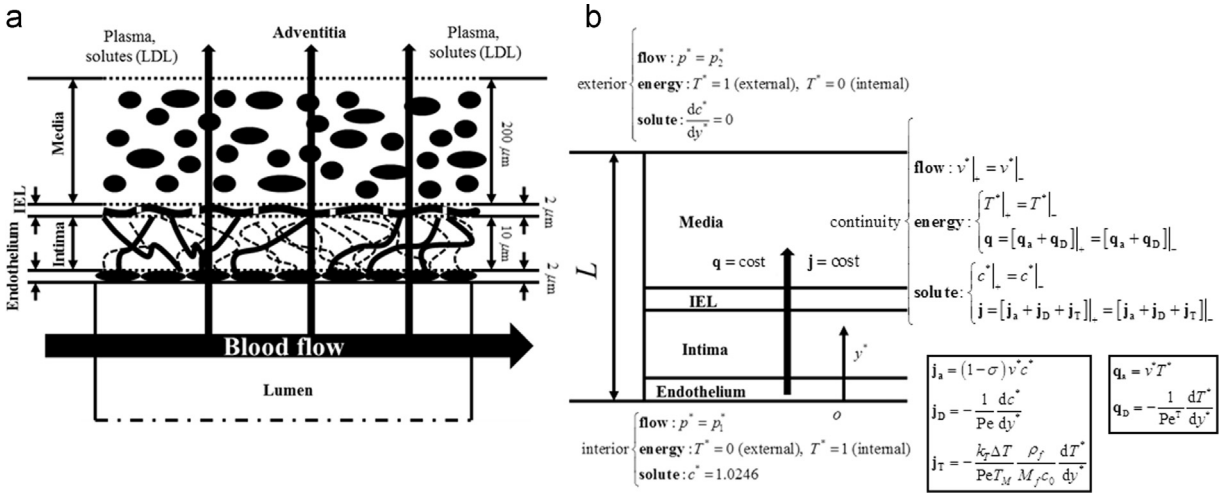

Fig. 1. (a) Anatomy of an artery and (b) boundary conditions.

"$<\ >$" and "$<\ >_f$" are referred to the extrinsic and intrinsic phase averaged value of a certain variable. These symbols will be dropped from now for simplicity.

The following well established results based on prior research works are invoked here:

- stationary state is assumed, due to the negligible effects of pulsatile flow (Yang and Vafai, 2006);
- convective term can be neglected (Vafai and Tien, 1981; Khaksour and Vafai, 2008; Wang and Vafai, 2013);
- Forchheimer term for the momentum equation, relative to the inertial coefficient f, is neglected due to the very low Reynolds number typical of the fluid flow through the arterial wall;
- osmotic pressure effects on the velocity in the arterial wall are considered to be negligible (Yang and Vafai, 2006; Chung and Vafai, 2014);
- Brinkman viscous effects term, relative to the solid boundaries, can be neglected (Yang and Vafai, 2008);
- Dufour effect can be neglected for hyperthermia effects on LDL transport (Chung and Vafai, 2014), and in general for liquids (Aouachria et al., 2012);

Utilizing the above established results based on the prior literature, the governing equations for the LDL transport within an arterial wall can be presented as:

$$\nabla \cdot \mathbf{v} = 0 \tag{7}$$

$$\nabla p = -\frac{\mu_f}{K}\mathbf{v} \tag{8}$$

$$(1-\sigma_S)\mathbf{v}\cdot\nabla c = D_{eff}\nabla^2 c + \frac{k_T\rho_f}{M_f}\frac{D_{eff}}{T}\nabla^2 T - kc \tag{9}$$

$$\mathbf{v}\cdot\nabla T = \alpha_{eff}\nabla^2 T \tag{10}$$

3. Analytical solution

3.1. Dimensionless governing equations and boundary conditions

Governing Eqs. (7)–(10) are further simplified by observing the following attributes established in earlier literature:

- filtration velocity in the axial direction is much smaller than filtration velocity in the radial direction. This means that LDL transport can be approximated as independent of axial direction (Yang and Vafai, 2006; Yang and Vafai, 2008);
- heat transfer is independent of axial direction (Chung and Vafai, 2014; Iasiello et al., 2015);
- effect of curvature is negligible, since the thickness of the arterial wall is small when compared to the overall radius of the artery (Wang and Vafai, 2015).
- in the denominator of the Ludwig-Soret term, for each layer a mean temperature is considered. This simplification is justified and often appears in numerical and analytical studies (Alam and Rahman, 2006) for phenomena in which Ludwig-Soret effect is involved.

As such, the above equations can be written in a dimensionless form, resulting in:

$$\frac{dv^*}{dy^*} = 0 \tag{11}$$

$$\frac{dp^*}{dy^*} = -\frac{1}{\mathrm{ReDa}}v^* \tag{12}$$

$$(1-\sigma_S)v^*\frac{dc^*}{dy^*} = \frac{1}{\mathrm{Pe}}\frac{d^2c^*}{dy^{*2}} + \frac{k_T\Delta T}{\mathrm{Pe}T_M}\frac{\rho_f}{M_f c_0}\frac{d^2T^*}{dy^{*2}} - \frac{kL_0}{v_0}c^* \tag{13}$$

$$v^*\frac{dT^*}{dy^*} = \frac{1}{\mathrm{Pe}^{\mathrm{T}}}\frac{d^2T^*}{dy^{*2}} \tag{14}$$

where the following dimensionless parameters were used:

$$v^* = \frac{v}{v_0};\ c^* = \frac{c}{c_0};\ p^* = \frac{p}{\rho_f v_0^2};\ y^* = \frac{y}{L_0};\ \mathrm{Re} = \frac{\rho_f v_0 L_0}{\mu_f};\ \mathrm{Da} = \frac{K}{L_0^2};$$
$$\mathrm{Pe} = \frac{v_0 L_0}{D_{eff}};\ \mathrm{Pe}^{\mathrm{T}} = \frac{v_0 L_0}{\alpha_{eff}};\ T^* = \frac{T-T_c}{T_h-T_c}$$

where T_M is the mean temperature, Re the Reynolds number, Da the Darcy number, Pe the mass Peclet number, Pe^{T} the thermal Peclet number, v_0 the reference filtration velocity, set as $2.31\cdot10^{-8}$ m/s from Meyer et al. (1996), c_0 the reference concentration value at the lumen inlet section, namely $28.6\cdot10^{-3}$ mol/m^3 (Chung and Vafai, 2012) and L_0 is the reference length of the arterial wall, in the radial direction, namely 214 μm. T_h represents the temperature at the hot surface, and T_c the temperature at the cold surface.

Boundary conditions for Eqs. (11)–(14) are shown in Fig. 1b. For the flow, physiological transmural pressure conditions are considered with $\Delta p = 70$ mmHg (Meyer et al., 1996), with $p_1^* = p_1/\rho_f v_0^2$ and $p_2^* = p_2/\rho_f v_0^2$, where $p_1 = 100$ mmHg and $p_2 = 30$ mmHg. For the LDL, at the lumen/endothelium interface a value of $c^* = 1.0246$ is imposed (Yang and Vafai, 2006 and Yang and Vafai, 2008). This value corresponds to the LDL concentration at the midsection longitudinally of the lumen/endothelium interface (Yang and Vafai, 2006). Continuity conditions are employed at the boundaries between the different layers.

Thermophysical properties that close Eqs. (11)–(14) are the same that have been used by Chung and Vafai (2014) and Iasiello et al. (2015). In this study, also other thermophysical properties are employed for comparisons. However, we have mentioned when properties different from the above cited sources have been employed, by citing the literature source.

3.2. Fluid flow

Filtration velocity of the flow is obtained by means of a hydraulic analogy. Considering L* as the dimensionless thickness of each ith-layer $L^{i,*} = L^i/L_0$, filtration velocity is expressed in terms of (Yang and Vafai, 2008):

$$v^* = \frac{p_1^* - p_2^*}{\sum_{i=1}^{4} R^i} = \frac{p_1^* - p_2^*}{R^{end} + R^{int} + R^{IEL} + R^{med}} \tag{15}$$

with the i-layer hydraulic resistance R^i equal to:

$$R^i = \frac{L^{i,*}}{\mathrm{ReDa}} \tag{16}$$

Comparisons with results from literature are carried out in Fig. 2. Filtration velocity is reported as a function of axial coordinate, because models from literature are considered to be axisymmetric. In Fig. 2a, comparisons with numerical results from Yang and Vafai (2006), Ai and Vafai (2006), and Chung and Vafai (2012), is reported for physiological transmural pressure, while a comparison with numerical results from Yang and Vafai (2006), is carried out for different hypertensive transmural pressure values in Fig. 2b. It is shown that hypertension increases filtration velocity, as depicted in Eq. (15). A good agreement has been found with literature data for all cases.

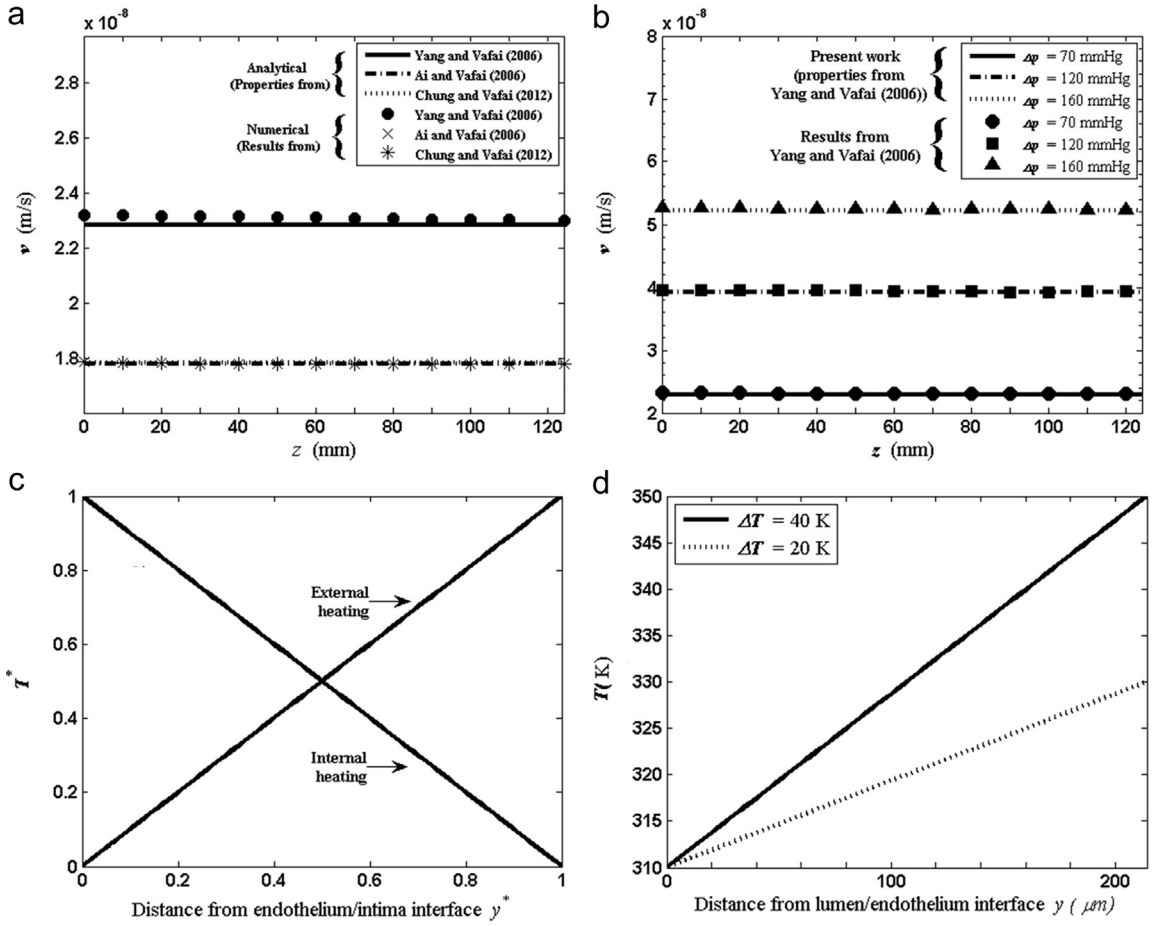

Fig. 2. Filtration velocity at the lumen/endothelium interface along the axial direction for (a) different set of properties, and (b) under hypertension conditions. (c) Dimensionless and (d) dimensional temperature profiles: the dimensional profile is for external heating, for $\Delta T =$ 20 K and 40 K.

3.3. Heat transfer

In order to solve concentration Eq. (13) to obtain the LDL concentration distribution, the energy Eq. (14) needs to be solved first. Once the temperature distribution is obtained, it will be utilized in the concentration Eq. (13).

The temperature distribution is obtained as:

$$T^*(y^*) = c_1^T e^{\lambda_1^T y^*} + c_2^T \tag{17}$$

This function is relative to each layer, and continuity between each layer is guaranteed by boundary conditions. Coefficients c_1^T and c_2^T are obtained by applying boundary conditions reported in Fig. 1b, resulting in a linear system with 8 equations and 8 unknowns. With references to Chung and Vafai (2014), the thermal diffusivity α_{eff} is chosen to be the same in each porous layer. This implies that $\mathrm{Pe}^{T,\mathrm{end}} = \mathrm{Pe}^{T,\mathrm{int}} = \mathrm{Pe}^{T,\mathrm{IEL}} = \mathrm{Pe}^{T,\mathrm{med}} = \mathrm{Pe}^{\mathrm{T}}$. Because Pe^{T} is chosen to be the same for each layer, it is possible to simplify this linear system to two equations with 2 unknowns. For the internal heating, we have:

$$\begin{cases} c_1^T = \frac{1}{1-e^{\lambda_1^T}} \\ c_2^T = -\frac{e^{\lambda_1^T}}{1-e^{\lambda_1^T}} \end{cases} \Rightarrow \begin{cases} c_1^T = -3.73 \cdot 10^4 \\ c_2^T = 3.73 \cdot 10^4 \end{cases} \tag{18}$$

while, for the external heating:

$$\begin{cases} c_1^T = -\frac{1}{1-e^{\lambda_1^T}} \\ c_2^T = \frac{1}{1-e^{\lambda_1^T}} \end{cases} \Rightarrow \begin{cases} c_1^T = 3.73 \cdot 10^4 \\ c_2^T = -3.73 \cdot 10^4 \end{cases} \tag{19}$$

The difference between internal and external heating is due to the physical location of the thermal load shown in Fig. 1b.

Results are reported in Figs. 2c and d. It is shown that temperature profiles are practically linear, as reported in the comprehensive numerical results from Chung and Vafai (2014) and Iasiello et al. (2015), where all the effects were accounted for, due to the small thermal Peclet numbers (Pe^{T}). External heating temperature profiles are reported for different ΔT s along the arterial wall in Fig. 2d.

3.4. Solute transport

Eq. (13) can be rearranged in order to obtain the following form:

$$\frac{1}{\mathrm{Pe}}\frac{\mathrm{d}^2c^*}{\mathrm{d}y^{*2}} - (1-\sigma_S)v^*\frac{\mathrm{d}c^*}{\mathrm{d}y^*} - \frac{kL_0}{v_0}c^* = -\frac{k_T\Delta T}{\mathrm{Pe}T_M}\frac{\rho_f}{M_f c_0}\frac{\mathrm{d}^2T^*}{\mathrm{d}y^{*2}} \tag{20}$$

Substituting the right term of this equation with the second derivative of Eq. (17), we obtain the following:

$$\frac{1}{\mathrm{Pe}}\frac{\mathrm{d}^2c^*}{\mathrm{d}y^{*2}} - (1-\sigma_S)v^*\frac{\mathrm{d}c^*}{\mathrm{d}y^*} - \frac{kL_0}{v_0}c^* = -\frac{k_T\Delta T}{\mathrm{Pe}T_M}\frac{\rho_f}{M_f c_0}c_1^T v^{*2}\mathrm{Pe}^{\mathrm{T}^2}e^{v^*\mathrm{Pe}^{\mathrm{T}}y^*} \tag{21}$$

The solution for Eq. (21) can be presented as:

$$c^*(y^*) = c_1^i e^{\lambda_1 y^*} + c_2^i e^{\lambda_1 y^*} + A^i e^{\lambda_1^T y^*} \tag{22}$$

where i refers to the ith-layer. Eigenvalues λ_1 and λ_2 are:

$$\lambda_{1,2} = \frac{\mathrm{Pe}(1-\sigma_S)v^* \pm \sqrt{[\mathrm{Pe}(1-\sigma_S)v^*]^2 + 4\frac{k\mathrm{Pe}L_0}{v_0}}}{2} \tag{23}$$

Eigenvalues for endothelium, intima and IEL are obtained by setting $k=0$. It is straightforward to show that, in these three layers, $\lambda_2=0$. The A^i is given by:

$$A^i=-\left[\frac{k_T\Delta T}{T_M}\frac{\rho_f}{M_f c_0}c_1^T\right]\cdot\frac{1}{1-\mathrm{Le}(1-\sigma_S)-\frac{kL_0\mathrm{Le}}{v_0 v^{*2}\mathrm{Pe}^{\mathrm{T}}}} \tag{24}$$

where the Lewis number is defined as $\mathrm{Le}=\mathrm{Pe}/\mathrm{Pe}^{\mathrm{T}}$. Continuity between layers is guaranteed by boundary conditions reported in Fig. 1b. Constants c_1^i and c_2^i are obtained, for each ith-layer, by applying such boundary conditions to Eq. (22), obtaining the following 8 equations in 8 unknowns:

$$c_1^{end}+c_2^{end}+A^{end}=1.0246 \tag{25a}$$

$$c_1^{end}e^{\lambda_1^{end}y^{*,end}}+c_2^{end}+A^{end}e^{v^*\mathrm{Pe}^{\mathrm{T}}y^{*,end}}=c_1^{int}e^{\lambda_1^{int}y^{*,end}}+c_2^{end}+A^{end}e^{v^*\mathrm{Pe}^{\mathrm{T}}y^{*,end}} \tag{25b}$$

$$\begin{aligned}&\left[\left(1-\sigma_S^{end}\right)\right]v^*\left(c_1^{end}e^{\lambda_1^{end}y^{*,end}}+c_2^{end}+A^{end}e^{v^*\mathrm{Pe}^{\mathrm{T}}y^{*,end}}\right)\\&-\frac{1}{\mathrm{Pe}^{\mathrm{end}}}\left(\lambda_1^{end}c_1^{end}e^{\lambda_1^{end}y^{*,end}}+A^{end}v^*\mathrm{Pe}^{\mathrm{T}}e^{v^*\mathrm{Pe}^{\mathrm{T}}y^{*,end}}\right)-\\&-\frac{k_T\Delta T}{\mathrm{Pe}^{\mathrm{end}}T_M^{end}}\frac{\rho_f}{M_f c_0}v^*\mathrm{Pe}^{\mathrm{T}}c_1^Te^{v^*\mathrm{Pe}^{\mathrm{T}}y^{*,end}}\\&=\left[\left(1-\sigma_S^{int}\right)\right]v^*\left(c_1^{int}e^{\lambda_1^{int}y^{*,end}}+c_2^{int}+A^{int}e^{v^*\mathrm{Pe}^{\mathrm{T}}y^{*,end}}\right)-\\&-\frac{1}{\mathrm{Pe}^{\mathrm{int}}}\left(\lambda_1^{int}c_1^{int}e^{\lambda_1^{int}y^{*,end}}+A^{int}v^*\mathrm{Pe}^{\mathrm{T}}e^{v^*\mathrm{Pe}^{\mathrm{T}}y^{*,end}}\right)\\&-\frac{k_T\Delta T}{\mathrm{Pe}^{\mathrm{int}}T_M^{int}}\frac{\rho_f}{M_f c_0}v^*\mathrm{Pe}^{\mathrm{T}}c_1^Te^{v^*\mathrm{Pe}^{\mathrm{T}}y^{*,end}}\end{aligned} \tag{25c}$$

$$c_1^{int}e^{\lambda_1^{int}y^{*,\ int}}+c_2^{int}+A^{int}e^{v^*\mathrm{Pe}^{\mathrm{T}}y^{*,\ int}}=c_1^{iel}e^{\lambda_1^{IEL}y^{*,\ int}}+c_2^{IEL}+A^{IEL}e^{v^*\mathrm{Pe}^{\mathrm{T}}y^{*,\ int}} \tag{25d}$$

$$\begin{aligned}&\left[\left(1-\sigma_S^{int}\right)\right]v^*\left(c_1^{int}e^{\lambda_1^{int}y^{*,\ int}}+c_2^{int}+A^{int}e^{v^*\mathrm{Pe}^{\mathrm{T}}y^{*,\ int}}\right)\\&-\frac{1}{\mathrm{Pe}^{\mathrm{int}}}\left(\lambda_1^{int}c_1^{int}e^{\lambda_1^{int}y^{*,\ int}}+A^{int}v^*\mathrm{Pe}^{\mathrm{T}}e^{v^*\mathrm{Pe}^{\mathrm{T}}y^{*,\ int}}\right)-\\&-\frac{k_T\Delta T}{\mathrm{Pe}^{\mathrm{int}}T_M^{int}}\frac{\rho_f}{M_f c_0}v^*\mathrm{Pe}^{\mathrm{T}}c_1^Te^{v^*\mathrm{Pe}^{\mathrm{T}}y^{*,\ int}}\\&=\left[\left(1-\sigma_S^{IEL}\right)\right]v^*\left(c_1^{IEL}e^{\lambda_1^{IEL}y^{*,\ int}}+c_2^{IEL}+A^{IEL}e^{v^*\mathrm{Pe}^{\mathrm{T}}y^{*,\ int}}\right)-\\&-\frac{1}{\mathrm{Pe}^{IEL}}\left(\lambda_1^{IEL}c_1^{IEL}e^{\lambda_1^{IEL}y^{*,\ int}}+A^{IEL}v^*\mathrm{Pe}^{\mathrm{T}}e^{v^*\mathrm{Pe}^{\mathrm{T}}y^{*,\ int}}\right)\\&-\frac{k_T\Delta T}{\mathrm{Pe}^{IEL}T_M^{IEL}}\frac{\rho_f}{M_f c_0}v^*\mathrm{Pe}^{\mathrm{T}}c_1^Te^{v^*\mathrm{Pe}^{\mathrm{T}}y^{*,\ int}}\end{aligned} \tag{25e}$$

$$c_1^{IEL}e^{\lambda_1^{IEL}y^{*,IEL}}+c_2^{IEL}+A^{IEL}e^{v^*\mathrm{Pe}^{\mathrm{T}}y^{*,IEL}}=c_1^{med}e^{\lambda_1^{med}y^{*,IEL}}+c_2^{med}+A^{med}e^{v^*\mathrm{Pe}^{\mathrm{T}}y^{*,IEL}} \tag{25f}$$

$$\begin{aligned}&\left[\left(1-\sigma_S^{IEL}\right)\right]v^*\left(c_1^{IEL}e^{\lambda_1^{IEL}y^{*,IEL}}+c_2^{IEL}+A^{IEL}e^{v^*\mathrm{Pe}^{\mathrm{T}}y^{*,IEL}}\right)\\&-\frac{1}{\mathrm{Pe}^{IEL}}\left(\lambda_1^{IEL}c_1^{IEL}e^{\lambda_1^{IEL}y^{*,IEL}}+A^{IEL}v^*\mathrm{Pe}^{\mathrm{T}}e^{v^*\mathrm{Pe}^{\mathrm{T}}y^{*,IEL}}\right)-\\&-\frac{k_T\Delta T}{\mathrm{Pe}^{IEL}T_M^{IEL}}\frac{\rho_f}{M_f c_0}v^*\mathrm{Pe}^{\mathrm{T}}c_1^Te^{v^*\mathrm{Pe}^{\mathrm{T}}y^{*,IEL}}\\&=\left[\left(1-\sigma_S^{med}\right)\right]v^*\left(c_1^{med}e^{\lambda_1^{med}y^{*,IEL}}+c_2^{med}+A^{med}e^{v^*\mathrm{Pe}^{\mathrm{T}}y^{*,IEL}}\right)-\\&-\frac{1}{\mathrm{Pe}^{med}}\left(\lambda_1^{med}c_1^{med}e^{\lambda_1^{med}y^{*,IEL}}+\lambda_2^{med}c_2^{med}e^{\lambda_2^{med}y^{*IEL}}+A^{med}v^*\mathrm{Pe}^{\mathrm{T}}e^{v^*\mathrm{Pe}^{\mathrm{T}}y^{*,IEL}}\right)\\&-\frac{k_T\Delta T}{\mathrm{Pe}^{med}T_M^{med}}\frac{\rho_f}{M_f c_0}v^*\mathrm{Pe}^{\mathrm{T}}c_1^Te^{v^*\mathrm{Pe}^{\mathrm{T}}y^{*,IEL}}\end{aligned} \tag{25g}$$

$$\lambda_1^{med}c_1^{med}e^{\lambda_1^{med}y^{*,IEL}}+\lambda_2^{med}c_2^{med}e^{\lambda_2^{med}y^{*,IEL}}+A^{med}v^*\mathrm{Pe}^{\mathrm{T}}e^{v^*\mathrm{Pe}^{\mathrm{T}}y^{*,IEL}}=0 \tag{25h}$$

where $y^{*,i}$ represents the value of the dimensionless coordinate y^*, with reference to the physical location of each ith-layer. In order to solve the aforementioned 8 equations in 8 unknowns, these are rearranged in a matrix form:

$$\mathbf{B}=\begin{bmatrix}1&1&0&0&0&0&0&0\\B_{2,1}&1&B_{2,3}&-1&0&0&0&0\\B_{3,1}&B_{3,2}&B_{3,3}&B_{3,4}&0&0&0&0\\0&0&B_{4,3}&1&B_{4,5}&-1&0&0\\0&0&B_{5,3}&-B_{3,4}&B_{5,5}&B_{5,6}&0&0\\0&0&0&0&B_{6,5}&1&B_{6,7}&B_{6,8}\\0&0&0&0&B_{7,5}&-B_{5,6}&B_{7,7}&B_{7,8}\\0&0&0&0&0&0&B_{8,7}&B_{8,8}\end{bmatrix}$$

$$\mathbf{g}=\begin{bmatrix}c_1^{end}\\c_2^{end}\\c_1^{int}\\c_2^{int}\\c_1^{IEL}\\c_2^{IEL}\\c_1^{med}\\c_2^{med}\end{bmatrix}\quad\mathbf{e}=\begin{bmatrix}1.0246-A^{end}\\\left(A^{int}-A^{end}\right)e^{v^*\mathrm{Pe}^{\mathrm{T}}y^{*,end}}\\E_{3,1}e^{v^*\mathrm{Pe}^{\mathrm{T}}y^{*,end}}\\\left(A^{IEL}-A^{int}\right)e^{v^*\mathrm{Pe}^{\mathrm{T}}y^{*,\ int}}\\E_{5,1}e^{v^*\mathrm{Pe}^{\mathrm{T}}y^{*,\ int}}\\\left(A^{med}-A^{IEL}\right)e^{v^*\mathrm{Pe}^{\mathrm{T}}y^{*,IEL}}\\E_{7,1}e^{v^*\mathrm{Pe}^{\mathrm{T}}y^{*,IEL}}\\E_{8,1}e^{v^*\mathrm{Pe}^{\mathrm{T}}y^{*,IEL}}\end{bmatrix} \tag{26}$$

where:

$$B_{2,1}=e^{\lambda_1^{end}y^{*,end}} \tag{27a}$$

$$B_{2,3}=-e^{\lambda_1^{int}y^{*,end}} \tag{27b}$$

$$B_{3,1}=\left[\left(1-\sigma_S^{end}\right)v^*-\frac{1}{Pe^{end}}\lambda_1^{end}\right]e^{\lambda_1^{end}y^{*,end}} \tag{27c}$$

$$B_{3,2}=\left(1-\sigma_S^{end}\right)v^* \tag{27d}$$

$$B_{3,3}=-\left[\left(1-\sigma_S^{int}\right)v^*-\frac{1}{Pe^{int}}\lambda_1^{int}\right]e^{\lambda_1^{int}y^{*,end}} \tag{27e}$$

$$B_{3,4}=-\left(1-\sigma_S^{int}\right)v^* \tag{27f}$$

$$B_{4,3}=e^{\lambda_1^{int}y^{*,\ int}} \tag{27g}$$

$$B_{4,5}=-e^{\lambda_1^{IEL}y^{*,\ int}} \tag{27h}$$

$$B_{5,3}=\left[\left(1-\sigma_S^{int}\right)v^*-\frac{1}{Pe^{int}}\lambda_1^{int}\right]e^{\lambda_1^{int}y^{*,\ int}} \tag{27i}$$

$$B_{5,5}=-\left[\left(1-\sigma_S^{IEL}\right)v^*-\frac{1}{Pe^{iel}}\lambda_1^{IEL}\right]e^{\lambda_1^{IEL}y^{*,\ int}} \tag{27j}$$

$$B_{5,6}=-\left(1-\sigma_S^{IEL}\right)v^* \tag{27k}$$

$$B_{6,5}=e^{\lambda_1^{IEL}y^{*,IEL}} \tag{27l}$$

$$B_{6,7}=-e^{\lambda_1^{med}y^{*,IEL}} \tag{27m}$$

$$B_{6,8}=-e^{\lambda_2^{med}y^{*,IEL}} \tag{27n}$$

$$B_{7,5}=\left[\left(1-\sigma_S^{IEL}\right)v^*-\frac{1}{Pe^{IEL}}\lambda_1^{IEL}\right]e^{\lambda_1^{IEL}y^{*,IEL}} \tag{27o}$$

$$B_{7,7}=-\left[\left(1-\sigma_S^{med}\right)v^*-\frac{1}{Pe^{med}}\lambda_1^{med}\right]e^{\lambda_1^{med}y^{*,IEL}} \tag{27p}$$

$$B_{7,8}=-\left[\left(1-\sigma_S^{med}\right)v^*-\frac{1}{Pe^{med}}\lambda_2^{med}\right]e^{\lambda_2^{med}y^{*,IEL}} \tag{27q}$$

$$B_{8,7} = \lambda_1^{med} e^{\lambda_1^{med} y^{*,med}} \tag{27r}$$

$$B_{8,8} = \lambda_2^{med} e^{\lambda_2^{med} y^{*,med}} \tag{27s}$$

$$E_{3,1} = e^{v^* Pe^T y^{*,end}} \left[\left(1-\sigma_S^{int}\right) v^* A^{int} - \frac{A^{int}}{Pe^{int}} v^* Pe^T - \frac{k_T \Delta T}{Pe^{int} T_M^{int}} \frac{\rho_f}{M_f c_0} v^* Pe^T c_1^T - \right.$$
$$\left. - \left(1-\sigma_S^{end}\right) v^* A^{end} - \frac{A^{end}}{Pe^{end}} v^* Pe^T - \frac{k_T \Delta T}{Pe^{end} T_M^{end}} \frac{\rho_f}{M_f c_0} v^* Pe^T c_1^T \right] \tag{27t}$$

$$E_{5,1} = e^{v^* Pe^T y^{*,\ int}} \left[(1-\sigma_S^{IEL}) v^* A^{IEL} - \frac{A^{IEL}}{Pe^{IEL}} v^* Pe^T - \frac{k_T \Delta T}{Pe^{IEL} T_M^{IEL}} \frac{\rho_f}{M_f c_0} v^* Pe^T c_1^T - \right.$$
$$\left. - \left(1-\sigma_S^{int}\right) v^* A^{int} - \frac{A^{int}}{Pe^{int}} v^* Pe^T - \frac{k_T \Delta T}{Pe^{int} T_M^{int}} \frac{\rho_f}{M_f c_0} v^* Pe^T c_1^T \right] \tag{27u}$$

$$E_{7,1} = e^{v^* Pe^T y^{*,IEL}} \left[\left(1-\sigma_S^{med}\right) v^* A^{med} - \frac{A^{med}}{Pe^{med}} v^* Pe^T \right.$$
$$- \frac{k_T \Delta T}{Pe^{med} T_M^{med}} \frac{\rho}{M_f c_0} v^* Pe^T c_1^T -$$
$$\left. - (1-\sigma_S^{IEL}) v^* A^{IEL} - \frac{A^{IEL}}{Pe^{IEL}} v^* Pe^T - \frac{k_T \Delta T}{Pe^{IEL} T_M^{IEL}} \frac{\rho_f}{M_f c_0} v^* Pe^T c_1^T \right] \tag{27v}$$

$$E_{8,1} = -A^{med} v^* Pe^T e^{v^* Pe^T y^{*,med}} \tag{27w}$$

The vector form of the coefficients **g** is obtained using the following matrix format:

$$\mathbf{g} = \mathbf{B}^{-1} \cdot \mathbf{e} \tag{28}$$

That is the compact form of the analytical solution of Eq. (13).

3.4.1. Comparisons for solute transport

3.4.1.1. Isothermal conditions. Comparisons with numerical results from Yang and Vafai (2006), Ai and Vafai (2006) and Chung and Vafai (2014), for the LDL transport for an isothermal arterial wall, are presented in Fig. 3. The corresponding properties utilized in each of the numerical results, which incorporate all the effects, were utilized in our analytical solution. A very good agreement with numerical results has been found for the present analytical solution. It is shown that the slope of concentration profile through the endothelium layer strongly depends on the set of properties employed. Indeed, the highest Pe^{end}, which indicates the competition between advective transport and diffusive transport, have been found in Chung and Vafai (2014), while the lowest in Yang and Vafai (2006).

A comparison with analytical solutions from Yang and Vafai (2008), Khakpour and Vafai (2008) and Wang and Vafai (2013) is reported in Fig. 4. Comparisons are reported for a physiological normal intramural pressure, namely $\Delta p = 70$ mmHg, with an endothelium diffusivity of $D_{eff}^{end} = 6 \times 10^{-17} \mathrm{m}^2/\mathrm{s}$ and for a hypertensive pressure, namely $\Delta p = 160$ mmHg, in which the endothelium diffusivity is taken as $D_{eff}^{end} = 2.4 \times 10^{-16} \mathrm{m}^2/\mathrm{s}$. The results are in very good agreement. It has to be observed that Yang and Vafai (2008) used a different value for the reaction term, namely $k = 1.4 \cdot 10^{-4}$ 1/s, instead of $k = 3.197 \cdot 10^{-4}$ 1/s.

3.4.1.2. Hyperthermia conditions. Our analytical results are compared with numerical results from Chung and Vafai (2014), for both external and internal hyperthermia loads, using the same thermo-diffusion coefficient and temperature differences that they had utilized, namely $k_T = 0$, 0.005, 0.01, and $\Delta T = 20$ K, 40 K. Such values were also used by Iasiello et al. (2015) for the study of

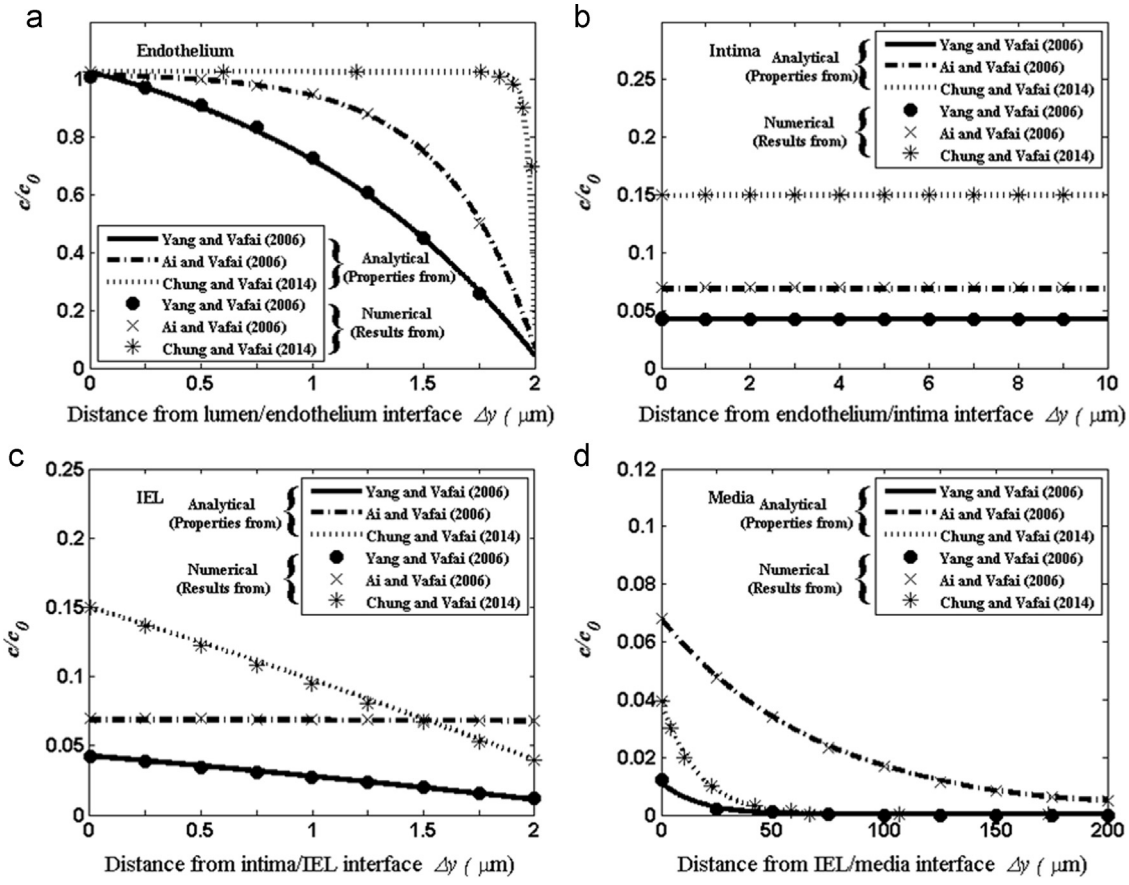

Fig. 3. Concentration profiles in different layers: (a) endothelium, (b) intima, (c) IEL and (d) media, without hyperthermia, compared with numerical solutions from literature.

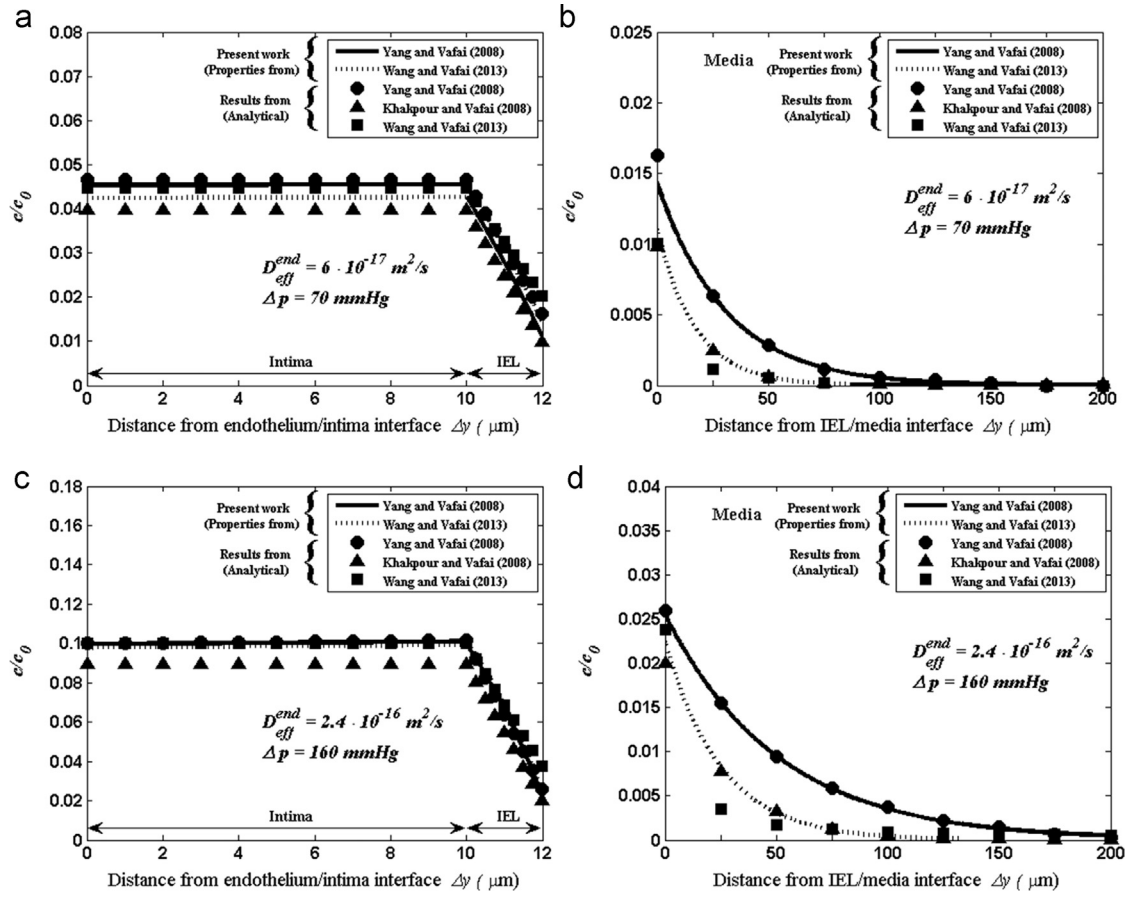

Fig. 4. Concentration profiles in different layers, without hyperthermia, compared with analytical solutions from literature: (a) intima and IEL, (b) media, both with $\Delta p = 70$mmHg and $D_{eff}^{end} = 6 \times 10^{-17}$m^2/s; (c) intima and IEL, (d) media, both with $\Delta p = 160$mmHg and $D_{eff}^{end} = 2.4 \times 10^{-16}$ m^2/s.

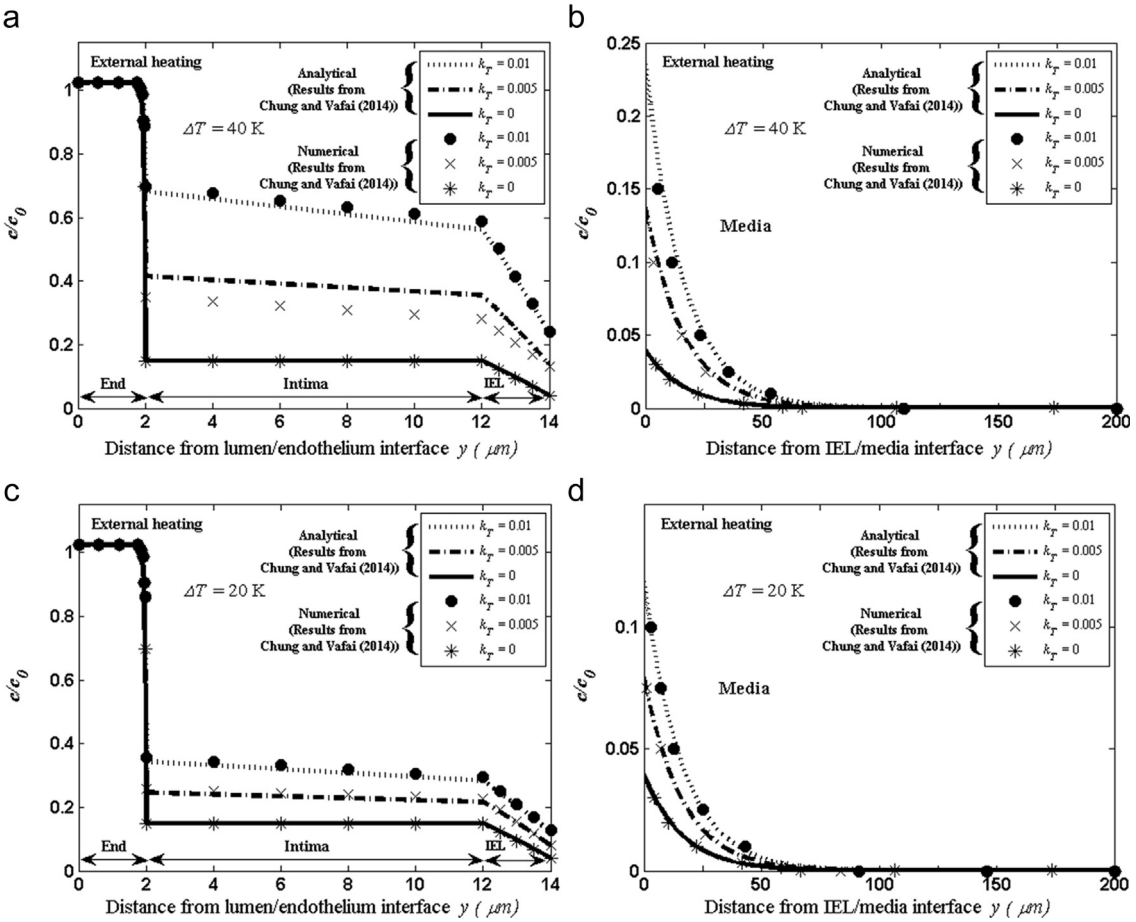

Fig. 5. Concentration profiles for different ΔTs under external heating: (a) and (b) are for ΔT= 40 K, while (c) and (d) are for ΔT= 20 K.

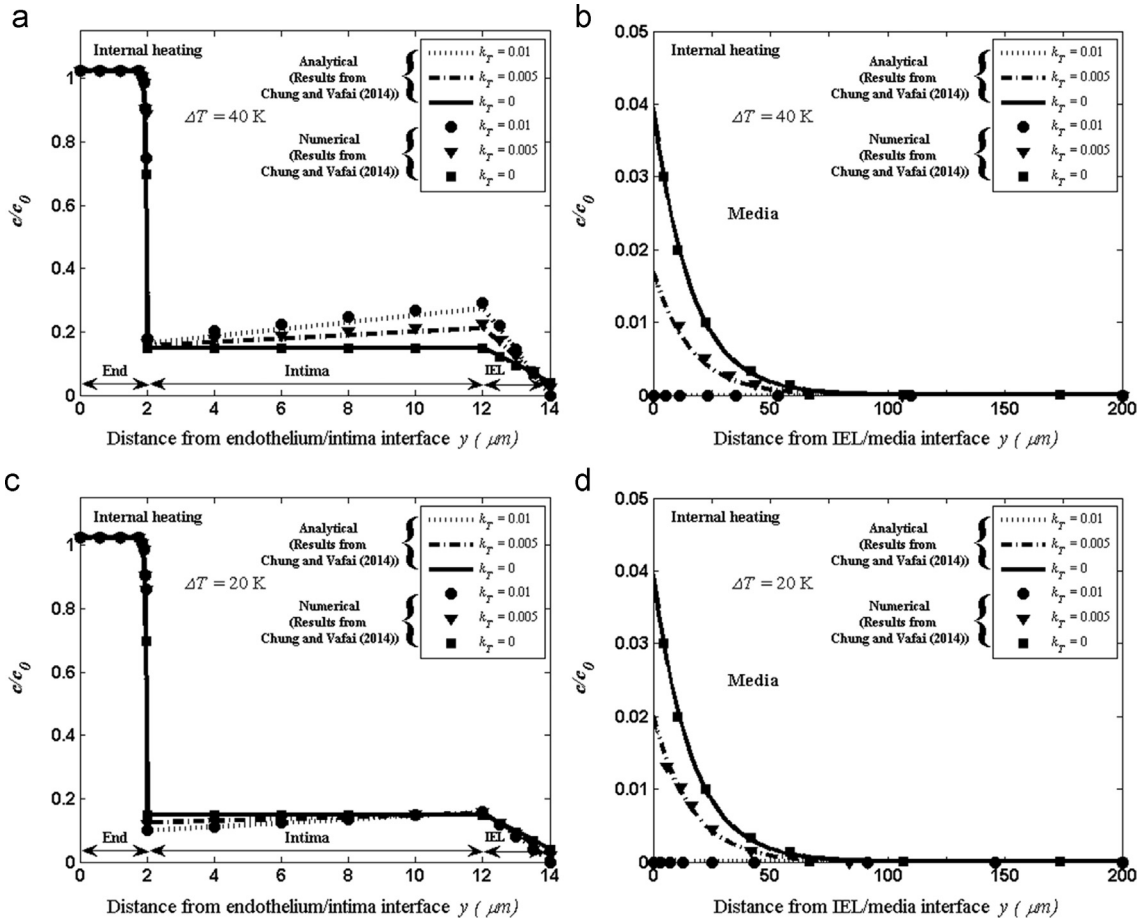

Fig. 6. Concentration profiles for different ΔTs under internal heating: (a) and (b) are for $\Delta T =$ 40 K, while (c) and (d) are for $\Delta T =$ 20 K.

hyperthermia effects on a stenosed artery. Thermo-diffusion coefficient k_T is usually about 0.01 (Chapman and Cowling, 1952; Wakeham et al., 1991, Chung and Vafai, 2014; Iasiello et al., 2015); however, because LDL is a heavy molecule, this value is expected to be lower. Comparisons for external heating are reported in Fig. 5, while for internal heating in Fig. 6. A good agreement can be observed. In the intima layer, this trend of the curves is justified by the fact that Ludwig-Soret effect moves the particles from the hot zone to the cold zone. This causes, in terms of LDL concentration, an accumulation of LDL on the endothelium/intima interface for external heating. For internal heating, LDL tends to accumulate on intima/IEL interface. As can be seen from Eq. (1), the absolute temperature value causes the concentration distribution to be in general higher in the intima for the external heating, compared to the internal heating case. Indeed, when heat is applied on the external wall, temperatures are lower in the intima region, compared to when heat is applied at the internal wall. As can be seen from the mass flux, a lower temperature value causes a reduction in the mass flux due to Ludwig-Soret effect $\mathbf{j_T}$. Finally, for the internal heating case shown in Fig. 6, the concentration tends to reduce in the other layers because other physical effects (molecular diffusion, advection, uptake of solutes) are more pronounced than Ludwig-Soret effect.

4. Analytical results

4.1. Hypertension effects under hyperthermia conditions

Hypertension effects under hyperthermia conditions are investigated here. Hypertension conditions are imposed by varying transmural pressure, such as $\Delta p = 70$, 120 and 160 mmHg, with $\Delta T =$ 40 K, for k_T values of 0, 0.005 and 0.01. Results are reported in Fig. 7 for external hyperthermia load, and in Fig. 8 for internal hyperthermia load.

Results on external heating show that hypertension generally increases LDL concentration in each layer. This effect is also amplified by hyperthermia. Indeed, the case with $k_T =$ 0.01 and $\Delta p =$ 160 mmHg has the highest concentration values, while when $k_T =$ 0 and $\Delta p =$ 70 mmHg concentration becomes the lowest. In the endothelium layer, the highest $\mathrm{Pe}^{\mathrm{end}}$ value corresponds to the case with $k_T =$ 0.01 and $\Delta p =$ 160 mmHg, which suggests that advection dominates diffusion substantially more than the other ones.

For the internal heating, similar to the external heating, LDL concentration in general increases in each layer with hypertension. For the endothelium layer, curves seem to have a similar slope. In the intima layer, hyperthermia generally reduces the concentration in the first part of the layer, but near the intima/IEL interface it gets always higher than the case with $k_T = 0$. This effect of reduction followed by an increase, is more emphasized for the hypertension conditions. Reduction of LDL in the IEL layer seems to be higher when Ludwig-Soret effect is more pronounced.

4.2. Effect of thermophysical properties

The effect of different properties on the hyperthermia effects is displayed in Fig. 9. In the endothelium layer, it can be seen that Ludwig-Soret effect has more influence on the LDL transport when properties from Yang and Vafai (2006) are used. In the intima layer, only absolute values of the curves are affected, while slopes

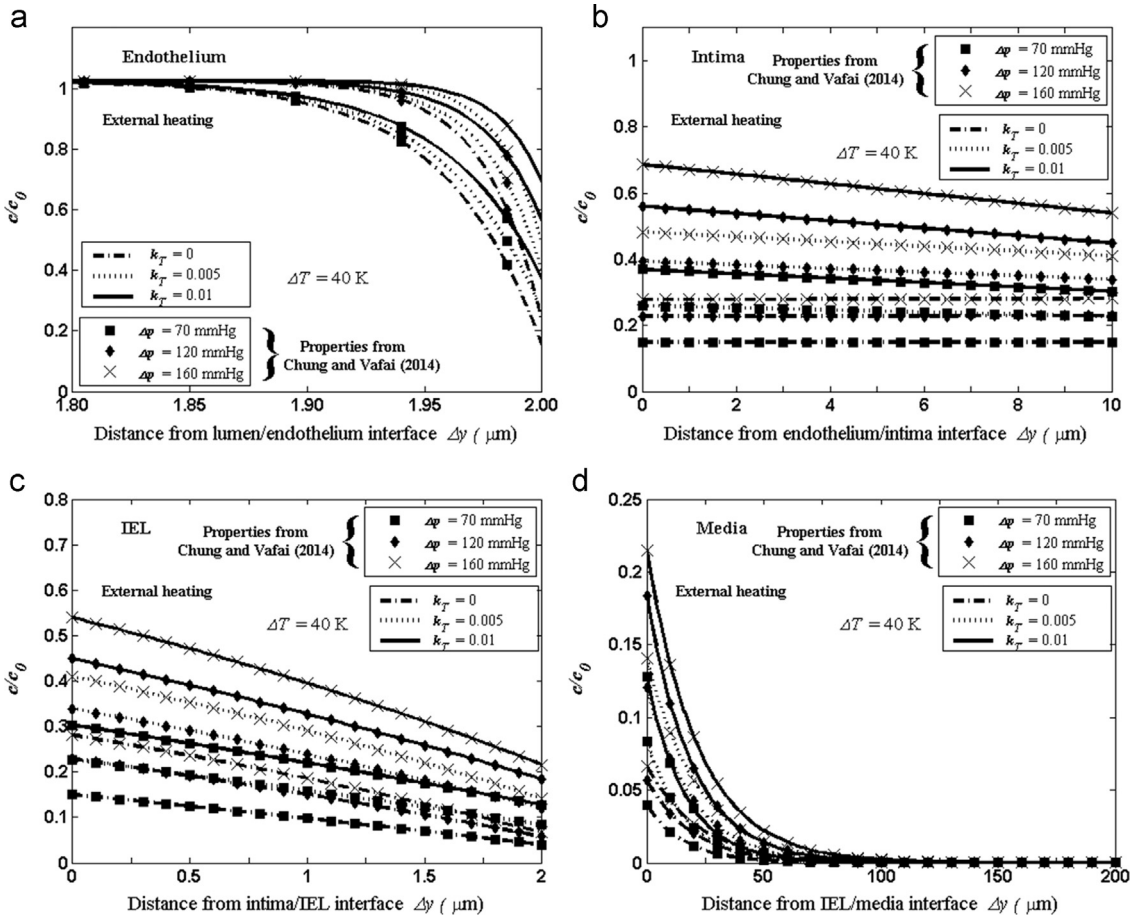

Fig. 7. Concentration profiles in different layers: (a) endothelium, (b) intima, (c) IEL and (d) media under external hyperthermia load, with hypertension effects, for $\Delta T = 40$ K.

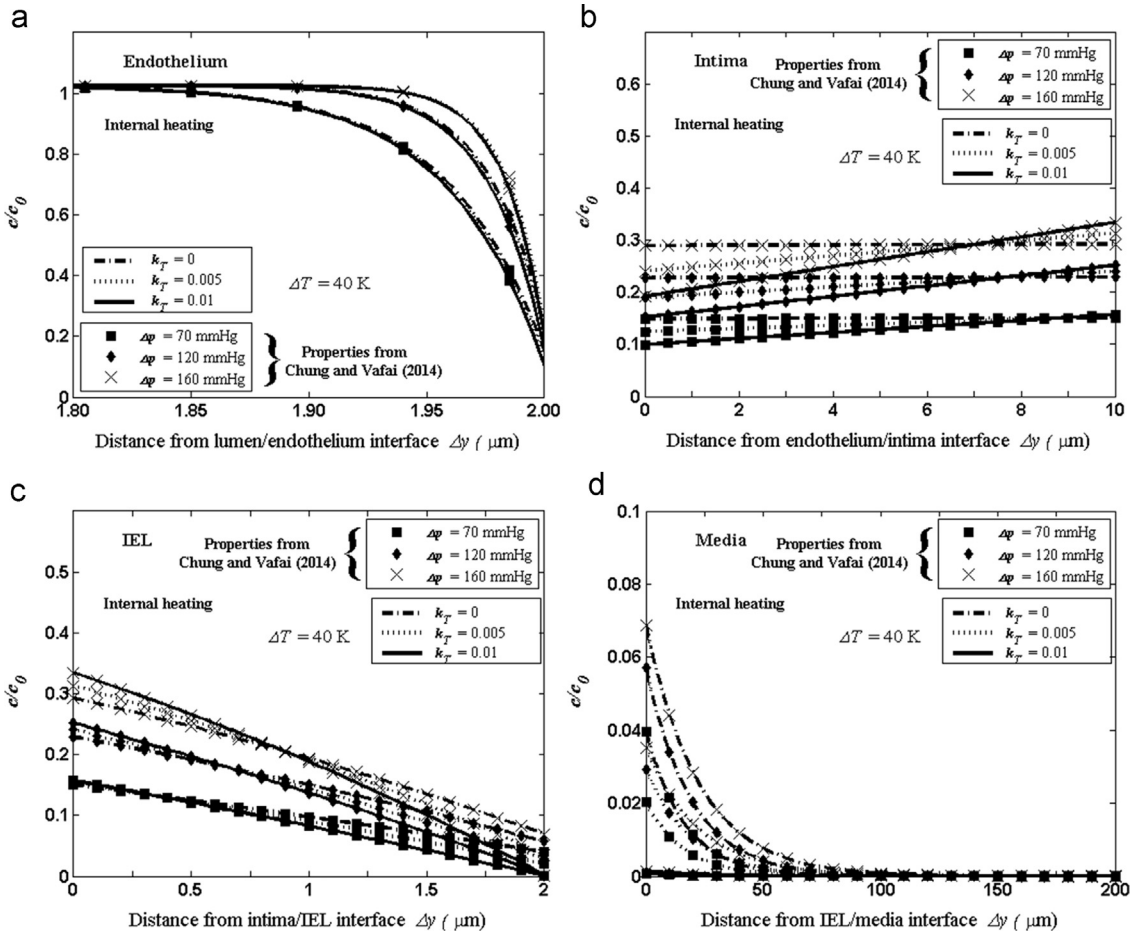

Fig. 8. Concentration profiles in different layers: (a) endothelium, (b) intima, (c) IEL and (d) media under internal hyperthermia load, with hypertension effects, for $\Delta T = 40$ K.

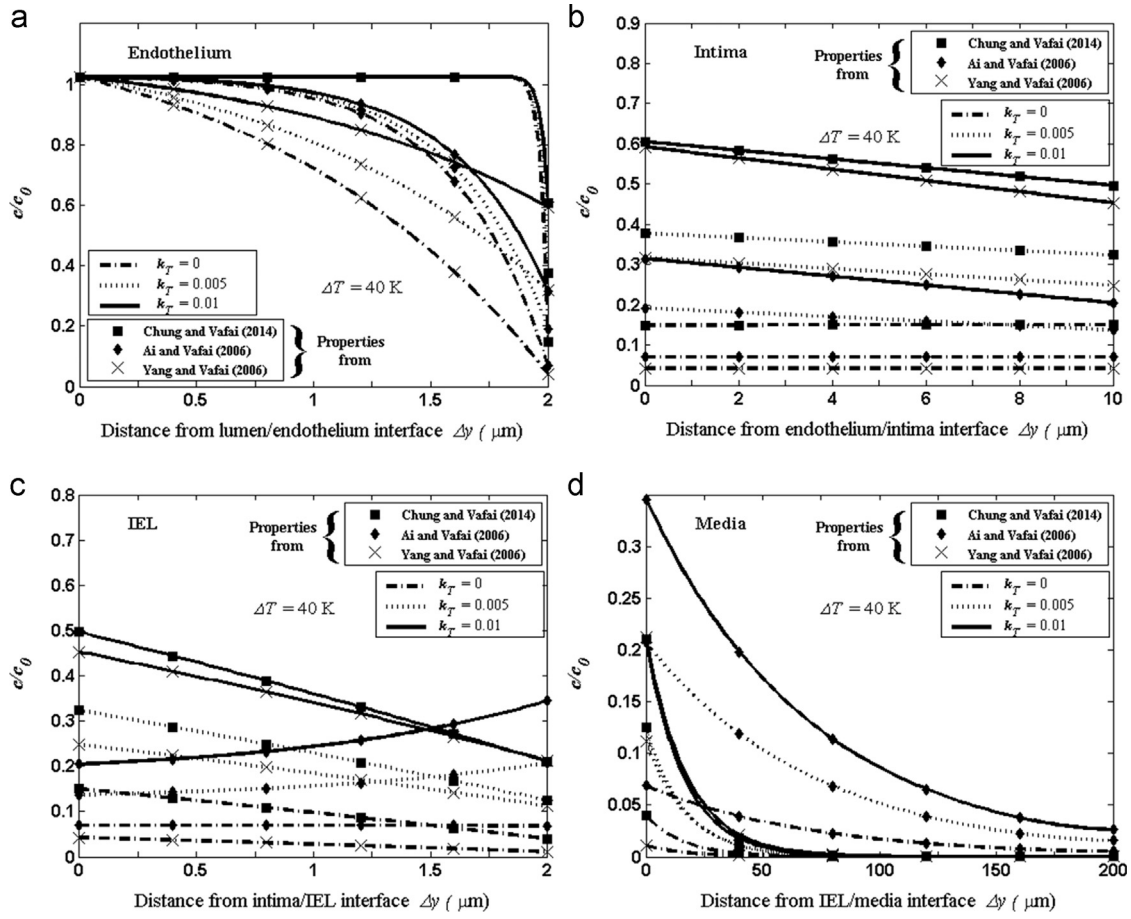

Fig. 9. Concentration profiles in different layers: (a) endothelium, (b) intima, (c) IEL and (d) media with external hyperthermia load, for $\Delta T = 40$ K, using different sets of physical properties.

under different k_T remain almost the same. In the IEL layer, properties from Chung and Vafai (2014) and from Ai and Vafai (2006) causes the LDL to have similar behavior, while the situation is different when properties from Ai and Vafai (2006) are utilized; in particular concentration increases, resulting in a concentration polarization effect on the IEL/media interface. The main reason for this is that Staverman reflection coefficient for the IEL layer taken from Ai and Vafai (2006) is about 15% less than Staverman reflection coefficient from the other two models. This causes the particles to accumulate on the IEL/media interface, when they are moving from media/adventitia interface to the intima/IEL interface due to the external heating application. Another reason is that first-order reaction term k used in Ai and Vafai (2006) transport model is one order of magnitude less than k used in the other two models.

4.3. Media/adventitia boundary condition effects

Effects of hyperthermia under different media/adventitia boundary conditions are shown in Fig. 10. These boundary conditions are $\partial c^*/\partial y^* = 0$, $c^* = 0$ and $c^* = 0.01$. Heat is applied by means of external heating, while $\Delta T = 40$ K and $k_T = 0.005$ or 0.01. It should be noted that $c^* = c/c_0$. As it can be seen, the media/adventitia boundary condition has an insignificant effect on the concentration distribution, except for a minor impact when the boundary condition $c^* = 0.01$ is employed. Comparing concentration profiles for $k_T = 0.005$ or 0.01 when boundary condition $c^* = 0.01$ is employed, it can be seen that these profiles are practically overlapped near the media/adventitia interface.

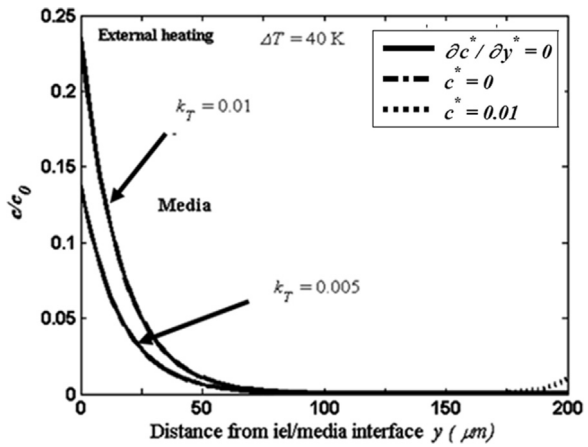

Fig. 10. Concentration profiles for the media layer by means of different boundary conditions at the media/adventitia interface, for $\Delta T = 40$ K and $k_T = 0.01$ or 0.005, under external heating.

5. Conclusions

An analytical solution has been presented for the problem of LDL transport through an arterial wall under hyperthermia conditions. Results are in very good agreement with previous numerical and analytical studies from literature for isothermal case, and also with numerical results when hyperthermia is considered. It is shown that hyperthermia generally increases LDL concentration through an arterial wall, and hypertension

combined with hyperthermia further augments this LDL accumulation. Effects of different sets of thermophysical properties are also discussed. An analysis of media/adventitia boundary condition is also carried out, showing that different boundary conditions have a negligible effect on LDL transport.

Conflict of Interest

There is no conflict of interest. This manuscript has not been submitted to anywhere else.

Acknowledgments

The stay of Marcello Iasiello at the University of California, Riverside was financially supported by UniNA and Compagnia di San Paolo, in the frame of Programme STAR.

References

Abraham, J.P., Gorman, J.M., Sparrow, E.M., Stark, J.R., Kohler, R.E., 2013. A mass transfer model of temporal drug deposition in artery walls. Int. J. Heat. Mass. Transf. 58, 632–638.
Abraham, J.P., Sparrow, E.M., Lovik, R.D., 2008. Unsteady, three-dimensional fluid mechanic analysis of blood flow in plaque-narrowed and plaque-freed arteries. Int. J. Heat. Mass. Transf. 51, 5633–5641.
Ai, L., Vafai, K., 2006. A coupling model for macromolecule transport in a stenosed arterial wall. Int. J. Heat. Mass. Transf. 49, 1568–1591.
Alam, M.S., Rahman, M.M., 2006. Dufour and Soret effects on mixed convection flow past a vertical porous flat plate with variable suction. Nonlinear Anal. Model. Control. 11, 3–12.
Alamiri, A., Khanafer, K., Vafai, K., 2014. Fluid-Structure Interactions in a Tissue during Hyperthermia. Numer. Heat. Tr. A-Appl. 66, 1–16.
Alazmi, B., Vafai, K., 2001. Analysis of fluid flow and heat transfer interfacial conditions between a porous medium and a fluid layer. Int. J. Heat. Mass. Transf. 44, 1735–1749.
Amiri, A., Vafai, K., 1994. Analysis of dispersion effects and non-thermal equilibrium, non-Darcian, variable porosity incompressible flow through porous media. Int. J. Heat. Mass. Transf. 37, 939–954.
Aouachria, Z., Rouichi, F., Haddad, D., 2012. Double Diffusion Effects on Convection in Flow on Vertical Plate Imbedded in Porous Media. FHMT 3, 023004.
Chapman, S., Cowling, T.G., 1952. The Mathematical Theory of Non-uniform Gases: An Account of the Kinetic Theory of Viscosity, Thermal Conduction and Diffusion in Gases. Cambridge University Press, Cambridge.
Chelikani, S., Sparrow, E.M., Abraham, J.P., Minkowycz, W.J., 2011. Mass Transfer in vascular access ports. Int. J. Heat. Mass. Transf. 54, 949–958.
Chung, S., Vafai, K., 2012. Effect of the fluid–structure interactions on low-density lipoprotein transport within a multi-layered arterial wall. J. Biomech. 45, 371–381.
Chung, S., Vafai, K., 2014. Mechanobiology of low-density lipoprotein transport within an arterial wall–impact of hyperthermia and coupling effects. J. Biomech. 47, 137–147.
Colton, C.K., Friedman, S., Wilson, D.E., Lees, R.S., 1972. Ultrafiltration of lipoproteins through a synthetic membrane. Implications for the filtration theory of atherogenesis. J. Clin. Invest. 51, 2472–2481.
Fry, D., 1985. Mathematical models of arterial transmural transport. Am. J. Physiol. 248, 240–263.
Hernàndez, J.I., Cepeda, M.F.J., Valdés, F., Guerrero, G.D., 2015. Microwave ablation: state-of-the-art review. Onco Targets Ther. 8, 1627–1632.
Huang, Z.J., Tarbell, J.M., 1997. Numerical simulation of mass transfer in porous media of blood vessel walls. Am. J. Physiol. 273, H464–H477.
Iasiello, M., Vafai, K., Andreozzi, A., Bianco, N., Tavakkoli, F., 2015. Effects of External and Internal Hyperthermia on LDL Transport and Accumulation Within an Arterial Wall in the Presence of a Stenosis. Ann. Biomed. Eng. 43, 1585–1599.
Ingle, S.E., Horne, F.H., 1973. The Dufour effect. J. Chem. Phys. 59, 5882–5894.
Kays, W.M., Crawford, M.E., 1993. Convective Heat and Mass Transfer. Mcgraw-Hill, New York.
Kedem, O., Katchalsky, A., 1958. Thermodynamic analysis of the permeability of biological membranes to non-electrolytes. Biochim. Biophys. Acta 27, 229–246.
Kenjereš, S., de Loor, A., 2014. Modelling and simulation of low-density lipoprotein transport through multi-layered wall of an anatomically realistic carotid artery bifurcation. J. R. Soc. Interface 11, 20130941.
Khakpour, M., Vafai, K., 2008. A Comprehensive Analytical Solution of Macromolecular Transport within an Artery. Int. J. Heat. Mass. Transf. 51, 2905–2913.
Liu, X., Fan, Y., Deng, X., 2011. Effect of the endothelial glycocalyx layer on arterial LDL transport under normal and high pressure. J. Theor. Biol. 283, 71–81.
Ludwig, C., 1856. Diffusion zwischen ungleich erwwärmten orten gleich zusammengestzter lösungen, Sitz. Ber. Akad. Wiss. Wien. Math.-Naturw. Kl. 20, 539.
Mahjoob, S., Vafai, K., 2009. Analytical characterization of heat transport through biological media incorporating hyperthermia treatment. Int. J. Heat. Mass. Transf. 52, 1608–1618.
McGowan, M.P., 2013. Emerging low-density lipoprotein (LDL) therapies: Management of severely elevated LDL cholesterol – The role of LDL-apheresis. J. Clin. Lipidol. 7, S21–S26.
Meyer, G., Merval, R., Tedqui, A., 1996. Effects of pressure-induced stretch and convection on low-density lipoprotein and albumin uptake in the rabbit aortic wall. Circ. Res. 79, 532–540.
Naughton, N.M., Plourde, B.D., Starke, J.R., Hodis, S., Abraham, J.P., 2014. Impacts of waveforms on the fluid flow, wall shear stress, and flow distribution in cerebral aneurysms and the development of a universal reduced pressure. J. Biomed. Sci. Eng. 7, 7–14.
Nield, D.A., Kuznetsov, A.V., 1999. Local thermal nonequilibrium effects in forced convection in a porous medium channel: a conjugate problem. Int. J. Heat. Mass. Transf. 42, 3245–3252.
Nield, D.A., Kuznetsov, A.V., 2001. The interaction of thermal nonequilibrium and heterogeneous conductivity effects in forced convection in layered porous channes. Int. J. Heat. Mass. Transf. 44, 4369–4373.
Platten, J.K., 2006. The Soret effect: a review of recent experimental results. J. Appl. Mech.-T. ASME 73, 5–15.
Prosi, M., Zunino, P., Perktold, K., Quarteroni, A., 2005. Mathematical and numerical models for transfer of low-density lipoproteins through the arterial walls: a new methodology for the model set up with applications to the study of disturbed lumenal flow. J. Biomech. 38, 903–917.
Roesch, M., Mueller-Huebenthal, B., 2015. Review: the role of hyperthermia in treating pancreatic tumors. Indian. J. Surg. Oncol. 6, 75–81.
Soares, P.I., Ferreira, I.M., Igreja, R.A., Novo, C.M., Borges, J.P., 2012. Application of hyperthermia for cancer treatment: recent patents review. Recent Pat. Anticancer. Drug. Discov. 7, 64–73.
Soret, C., 1879. Sur l'état d'équilibre que prend au point de vue de sa concentration une dissolution saline primitivement homohéne dont deux parties sont portées à des températures différentes. Arch. Sci. Phys. Nat. 2, 48–61.
Stangeby, D.K., Ethier, C.R., 2002. Computational analysis of coupled blood-wall arterial LDL transport. J. Biomech. Eng. 124, 1–8.
Stark, J.R., Gorman, J.M., Sparrow, E.M., Abraham, J.P., Kohler, R.E., 2013. Controlling the rate of penetration of a therapeutic drug into the wall of an artery by means of a pressurized balloon. J. Biomed. Sci. Eng. 6, 527–532.
Sun, B., Vallez, L.J., Plourde, B.D., Abraham, J.P., Stark, J.R., 2015. Influence of supporting tissue on the deformation and compliance of healthy and diseased arteries. J. Biomed. Sci. Eng. 8, 490–499.
Tarbell, J.M., 2003. Mass transport in arteries and the localization of atherosclerosis. Annu. Rev. Biomed. Eng. 5, 79–118.
Vafai, K., Tien, C.L., 1981. Boundary and inertia effects on flow and heat transfer in porous media. Int. J. Heat. Mass. Transf. 24, 195–203.
Wada, S., Karino, T., 2000. Computational study on LDL transfer from flowing blood to arterial walls. In: Yamaguchi, T. (Ed.), Clinical Application of Computational Mechanics to the Cardiovascular System. Springer Japan, Tokyo, pp. 157–173.
Wakeham, W.A., Nagashima, A., Sengers, J.V., 1991. Experimental Thermodynamics, Vol. III, Measurement of the transport properties of fluids. Blackwell Scientific Publications, Oxford.
Xie, X., Tan, J., Wei, D., Lei, D., Yin, T., Huang, J., Zhang, X., Qiu, J., Tang, C., Wang, G., 2013. In vitro and in vivo investigations on the effects of low-density lipoprotein concentration polarization and haemodynamics on atherosclerotic localization in rabbit and zebrafish. J. R. Soc. Interface 10, 20121053.
Wang, S., Vafai, K., 2013. Analysis of the Effect of Stent Emplacement on LDL Transport within an Artery. Int. J. Heat. Mass. Transf. 64, 1031–1040.
Wang, S., Vafai, K., 2015. Analysis of low-density lipoprotein (LDL) transport within a curved artery. Ann. Biomed. Eng. 43, 1571–1584.
Wang, K., Tavakkoli, F., Wang, S., Vafai, K., 2015. Analysis and analytical characterization of bioheat transfer during radiofrequency ablation. J. Biomech. 48, 930–940.
Yang, N., Vafai, K., 2006. Modeling of Low-Density Lipoprotein (LDL) transport in the artery—Effects of hypertension. Int. J. Heat. Mass. Transf. 49, 850–867.
Yang, N., Vafai, K., 2008. Low-Density Lipoprotein (LDL) transport in an artery—A simplified analytical solution. Int. J. Heat. Mass. Transf. 51, 497–505.